JOURNAL OF MATERIALS SCIENCE **34** (1999) 1261–1270

Use of zirconium diboride-copper as an electrode in plasma applications

S. NORASETTHEKUL, P. T. EUBANK, W. L. BRADLEY*, B. BOZKURT
*Departments of Chemical Engineering (77843-3122) and *Mechanical Engineering, Texas A&M University, College Station, TX 77843-3123, USA*
E-mail: Somchintana.Norasetthekul@vlsi.com

B. STUCKER
Department of Industrial and Manufacturing Engineering, University of Rhode Island, Kingston, RI 02881-0805, USA

Frequent replacement of electrodes, due to their high wear rate, is an undesired feature of most thermal plasma processes. Hence, the discovery of a high spark-resistive tool, ZrB_2-Cu, is of interest. Performance evaluation of this metal matrix ceramic (MMC) employed electrical discharge machining (EDM), where steel is used as the cathode workpiece and the MMC is used as the anode tool. Compared with the performance of copper and graphite tools, ZrB_2-Cu yields the highest workpiece removal rate, and the lowest tool wear rate at high plasma heat flux conditions, resulting in an extremely low wear ratio. Energy dispersive spectroscopy shows deposition of workpiece materials (Fe, Cr, Ni and S) on the ZrB_2-Cu surface after EDM. This is due to the difference between the surface temperature of the tool and the workpiece. Scanning electron microscopy and elemental mapping analysis reveal that the composite electrode erodes by a combination of dominant evaporation and melting of the metal phase, negligible melting and thermal spalling in the ceramic phase, quick refreezing of the metal phase back to the surface, and deposition of the workpiece (steel) on the tool surface. Most of the heat is conducted through the Cu phase, reducing thermal stress in the ceramic phase. This causes lower surface temperatures for the molten ZrB_2 matrix; hence, the Cu tends to refreeze quickly near the surrounding ceramic matrix.

1. Introduction

In recent years, thermal plasma technology has played an important role in the development of new materials such as fine powders and thin films; material conservation by coating and hard facing; material processing, such as plasma sintering, spheroidization, cutting and welding, melting, deposition and spraying; refining of materials by smelting or extracting one material from mixtures; and material decomposition, such as toxic wastes [1]. This is because thermal plasma technologies are more energy efficient, more productive and less damaging to the environment than non-thermal plasma ones. However, continuous operation in plasma-related processes is difficult to sustain due to the electrode's high wear rate and its loss of shape, resulting in frequent electrode replacement. Accordingly, the discovery of new materials that possess high resistivity to plasma sparks and/or arcs is of interest. Such discoveries will not only increase processing time but also reduce manufacturing cost.

Zirconium diboride-copper (ZrB_2-Cu) seems to be an excellent spark-resistive electrode material. Although ZrB_2 has high hardness (8 based on the mineralogical scale) and a high melting point (3300 K), its low thermal stress resistivity and poor thermal conductivity (24 $W\,m^{-1}\,K^{-1}$) hinder its utilization in plasma applications. To enhance the overall properties of this material, the addition of Cu is necessary. We would expect that when the plasma strikes the electrode surface, Cu melts and/or vaporizes before ZrB_2, because Cu has a high thermal conductivity (401 $W\,m^{-1}\,K^{-1}$) and low melting point (1358 K). Thus, excess heat is carried away from the surface by the Cu until the thermal stress on the ceramic decreases, when the spark is extinguished or when the arc/spark moves to another surface location. Although the metal melts and vaporizes initially, it tends to resolidify quickly back to the surface after spark has disappeared.

The research of Harry [2] supports our idea of increasing the operation time of plasma-related equipment. For a rotating arc controlled by an external magnetic field, he obtained optimal conditions for minimum electrode erosion by varying arc velocity, axial magnetic flux density, rotational frequency, cooling water flow rate and electrode wall thickness.

Although there is very little literature for ZrB_2-Cu, some work in zirconium-based materials has been reported. Low zirconium cathode erosion rates in an air

plasma torch was reported by Marotta [3]. Stable operation of the plasma torch for 50 h without changing the zirconium electrode was possible with an erosion depth of 3 mm. In addition, ZrB_2-based composites have been used in aerospace industry as reported by Fenter [4]. In the research of Ise *et al*. [5], dispersion plating of ZrB_2 was carried out in Cu plating baths, resulting in a new electrical contact material. This material has high electrical conductivity, thermal conductivity and resistance to heat and wear. The utilization of ZrB_2-Cu as a cutting tool was cited by Cheng and coworkers [6, 7] due to its low removal rate in an electrical discharge machine (EDM). This work also showed that ZrB_2-Cu has much lower wear rates when compared with ZrB_2, ZrB_2-Mo and ZrB_2-Si.

Our performance evaluation of ZrB_2-Cu electrodes employed EDM. EDM uses a concentrated heat source to raise the temperature of the workpiece to high values, where normally a metal melts and/or vaporizes while thermal spalling is induced in ceramics [8]. The heat source is from successive spark discharges in a dielectric liquid. No mechanical stresses are exerted on the cut material since there is no direct contact between cathode and anode electrodes. Consequently, EDM machines the material effectively, irrespective of material hardness and strength, as long as the material has an electrical resistivity below 100 Ω cm. Therefore, besides metals, EDM can be applied to most interstitial ceramics like certain carbides, borides, nitrides, silicides and composites having a conducting matrix such as ZrB_2-Cu in our case. Among non-traditional machining processes, EDM yields the highest material removal rate, the lowest tolerance, and comparable surface roughness and damage depth [9].

The following effects were studied: effect of discharge current and spark duration (on-time) on electrode performance, electrode and workpiece removal rate, wear ratio of the electrode to workpiece, and surface quality of workpiece and electrode. We compared the performance of ZrB_2-Cu with graphite and copper electrodes, which are normally used in the USA and Europe, respectively. We also studied the erosion mechanism of ZrB_2-Cu electrode to verify our hypothesis.

1.1. Overview of electrical discharge machining

The principal components of EDM are two electrodes, a cathode and an anode (cutting tool and workpiece), separated by a liquid dielectric. At the begining of EDM operation, a high voltage of about 200 V is applied across a narrow gap of typically about 20–300 μm (depending on current) between the two electrodes. This high voltage induces an electric field in the insulating dielectric that is present in the narrow gap. This causes conducting particles suspended in the dielectric to concentrate at the points of the strongest electric field, which in turn results in a bridge being formed between the electrodes. At the same time, negatively charged particles are emitted from the cathode and collide with neutral particles in the gap between the electrodes, forming electrons and positively charged particles. This dielectric breakdown process spreads at an explosive rate,

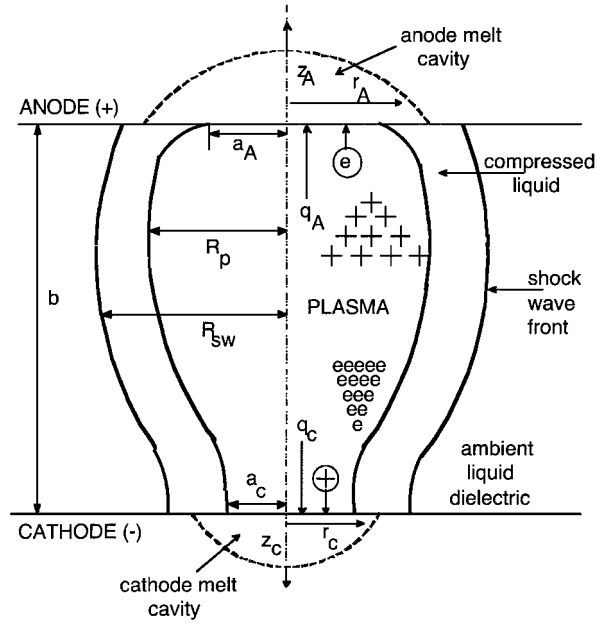

Figure 1 Schematic diagram of the EDM process showing circular heat sources, plasma configuration and melt cavities after a certain on-time.

resulting in the formation of a conducting channel between the electrodes, called plasma channel. Because this channel now conducts electricity between the two electrodes, the voltage, V, drops from 200 V to approximately 25 V within 1–3 μs and the current, I, increases from zero to a constant value set by the operator. The channel grows with time, called on-time, τ, which is typically less than a 100 μs, as set by the operator. Unlike a gas plasma, the surrounding dense liquid dielectric restricts the growth of the plasma channel and thus concentrates the input energy, $VI\tau$, in a very small volume. Energy densities of up to 3 J mm^{-3} result, causing local plasma temperatures to reach as high as 60 000 K. Dynamic plasma pressures rise to as much as 10 kbar due mainly to inertial effects. Fig. 1 shows the shape of the plasma channel that exists during the on-time, which is caused partly by the viscosity of the dielectric fluid [10] and partly by differences between the sizes of the spark root at the anodic and cathodic surfaces.

During the on-time, the high thermal-energy plasma radiates energy to both electrode surfaces and the surrounding dielectric fluid. This radiated energy is conducted into the interior of the electrode, creating a melt zone for metal, and a thermal-spalled and/or melt zones for ceramics. Limited electrode vaporization occurs due to the high plasma pressures. The anode first begins to melt rapidly due to the absorption of fast moving electrons at the start of the pulse. However, after a few microseconds, it resolidifies back to the surface owing to the lateral movement of electrons at the anode surface. This lateral movement is due to electrons' light mass and causes an expansion of the plasma channel near the anode, resulting in a decrease in the local heat flux, q_A, at the anode surface [11]. The plasma radius at the anode surface changes with time as $a_A = a_{Ao}\tau^{3/4}$, where a_{Ao} is the spot size constant [12], resulting in an expanding heat source for conduction into the interior of the anode. Melting of the cathode is delayed in time compared with that of the anode due to lower mobility of the positive ions. However, both electrodes

receive considerable energy from thermal radiation, i.e. photon bombardment. Since the electrons are emitted from the cathode, the plasma radius at the cathode is much smaller, thereby approximating a point heat source for conduction into its interior [13]. In addition, the plasma radius, R_p, is found to be increased with on-time and is proportional to $\tau^{3/4}$. This time exponent of (3/4) was that found for the plasma radius by Robinson and coworkers [14–16], and was fitted to the wide-ranging experimental AGIE/SIT data, which were successfully correlated by the coauthors of this paper [17]. The plasma radius increases with time because: (i) the high internal plasma pressure is pushing back the high-density dielectric, and (ii) liquid dielectric is converted to plasma at the interface between the plasma and the dielectric as shown in Fig. 1.

At the end of the on-time, an off-time, δ, begins when the current is terminated to the machine. During this off-time, a violent collapse of the plasma channel and the vapour bubble occurs, causing superheated, molten liquid on the electrode's surface to explode into the liquid dielectric. While some of this material is flushed out by the flowing dielectric, the remainder of the melt in the cavities resolidifies in place, waiting removal by a later spark.

There are two types of EDM machines, the die-sinker and the wire machine. In our work, the die-sinker was used where the cathode is the workpiece and the anode serves as the shaping tool. It is desired to remove material from the workpiece, not the tool, and to use the tool repeatedly for the same applications. Consequently, the spark-resistive material should be used as the tool in order to burn its mirror-like shape (reverse image) into the workpiece with minimum dimension loss by the electrode.

2. Experimental procedure

2.1. Materials

We used EDM-100 fine graphite (POCO), alloy 110 copper (McMaster-Carr), type 303 stainless steel (McMaster-Carr), ZrB_2-Cu 1700 and ZrB_2-Cu ART as electrodes. The dimensions of all the above electrodes were $(9.525 \times 10^{-3}) \times (9.525 \times 10^{-3}) \times (6.35 \times 10^{-2})$ m. The Mechanical Engineering Department at Texas A&M University fabricated the ZrB_2-Cu 1700, whereas Advanced Refractory Technologies, Inc. (ART) manufactured ZrB_2-Cu ART. The polymer-coated powders of ZrB_2 were mechanically pressed with a pressure of 5333 psig for ZrB_2-Cu ART or 20 000 psig for ZrB_2-Cu 1700 to obtain a green body. This allowed the particles to be tacked together by the polymer. The coating polymer was Ceramer 1608 polymer binder (Petrolyte). Then, the green body was infiltrated by Cu and sintered in a furnace. The temperature of the furnace was approximately 1973 K, well above the melting point of Cu, allowing copper to melt and flow into the pores of the green body. At the same time, this high temperature burned the polymer out of the ceramic particles. After sintering, the furnace was cooled to ambient temperature to give a ZrB_2-Cu electrode with continuous phases of both ZrB_2 and Cu matrices. The copper used by ART has different trace elements compared with that used by Texas A&M University. The graphite has an average particle size of 11–20 μm, and is normally used in intermediate-graded EDM applications. The copper has a minimum purity of 99.9% and excellent corrosion resistance. The stainless steel is austentic, non-heatable, and of good resistance to corrosion. It contains at least 10% chromium and nickel, and trace amounts of sulfur and phosphorous, resulting in superb machining characteristics.

2.2. Machining procedures

An AGIETRON 1 U die-sinking machine was used to study the electrode performance. To maximize flushing efficiency, one end of the workpiece faced upwards to contact the tool surface, as shown in Fig. 2. The flushing of debris is accomplished by an up/down movement of the electrode. The dielectric fluid was British Petroleum (BP) cutting oil.

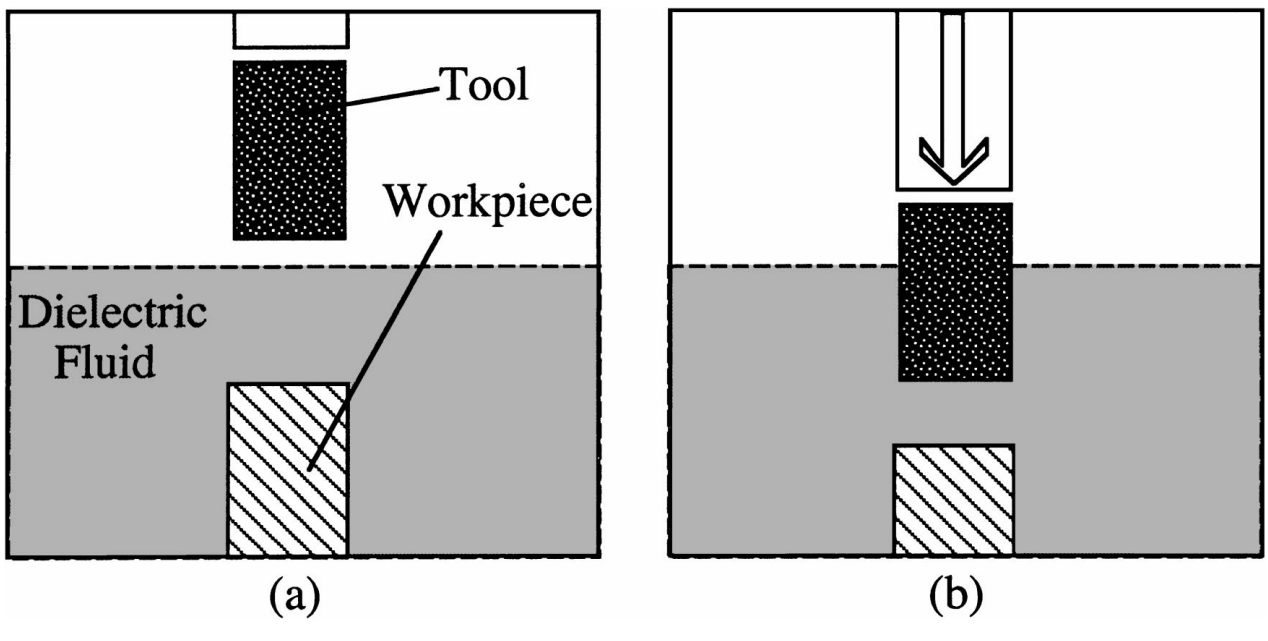

Figure 2 The configuration and setup of both tool and workpiece in the working tank of the die-sinker: (a) before EDM and (b) after EDM.

We used graphite, copper, ZrB_2-Cu ART and ZrB_2-Cu 1700 as anode tools, while steel was the cathode workpiece. The experimental conditions of EDM operation are nine different on-times ranging from 3.2 to 560 μs, six different currents ranging from 4.0 to 37.1 A, and a constant off-time of 100 μs. For graphite, copper and ZrB_2-Cu 1700 tools, all nine on-times were used at each current setting, except for a current of 4.0 A, resulting in a total of 45 experimental conditions. In addition, at least three repeated datum for each experimental condition were collected for these three tools. On the other hand, for ZrB_2-Cu ART, a current of 14.8 A with all nine on-times and a current of 4.0 A with an on-time of 3.2 μs were used. Only one run was conducted for each experimental condition for ZrB_2-Cu ART. The current, in our experiment, is defined as the constant value for each on-time. We stopped the machining process after the workpiece was cut for a vertical depth of 2.5 mm. The total experimental time for each run was varied depending on the material type, current and on-time. The experimental time was decreased with increasing on-time and current.

After each cutting, the EDM surface of the ZrB_2-Cu electrodes was ground using a B99 line DW mounted wheel (Norton). The surface of the wheel was covered with synthetic diamonds with a grit size of 150. Unlike for ZrB_2-Cu, a four-flute end mill (Putnam) was used to grind off the surface of copper, graphite and steel electrodes. The end mill was made of high-speed stainless steel. The electrodes, including ZrB_2-Cu, were then polished using a diamond bench stone with a grit size of 220. WD-40 lubricating oil was used in both the grinding and polishing steps. We used a new clean surface for each experiment to eliminate impurities and surface quality effect on wear rate, wear ratio and surface quality.

2.3. Electrode performance

Material removal rate is defined as the volume of material removed per total machining time. The total machining time is the sum of the on-time and off-time for each cycle of operation. The volume of material removed was determined by multiplying the surface area of the electrode by the depth of either the machined workpiece or tool. Wear ratio is equal to the tool removal rate divided by the workpiece removal rate.

2.4. Surface characterization

We used a Surfanalyzer 5000/400 surface analysis system (Federal Products Co.) to determine the roughness of the electrode surface. The measured roughness, Rq, is a geometric average [a root-mean-square (r.m.s.) value] of the measured roughness profile height deviation, y, taken within the specimen length, L, and measured from the mean line [18]. Rq is calculated from the following equation

$$Rq = \left(\frac{1}{L} \int_0^L |y^2| \, \mathrm{d}x \right)^{1/2}$$

$$\approx \left(\frac{y_1^2 + y_2^2 + y_3^2 + \cdots + y_n^2}{n} \right)^{1/2}$$

A Joel JSM-6400 scanning electron microscope (SEM) was used to visualize the cut surfaces. We performed elemental mapping, using a Cameca SX 50 electron microprobe, on the EDM surfaces. An energy dispersive spectrometer (EDX), a part of Cameca SX 50 system, was also used to analyse for elements present in particular areas under the microscope. The electron beam of this microprobe was used to excite X-rays from the specimen. The emitted X-rays were measured on the basis of their energies. The EDX processes the energy-proportional pulses produced by a solid-state detectors (Li-drifted silicon), sorts them according to their energy using a 2000-channel analyser, and counts the pulse produced in a series of amplitude ranges appropriate to the elements sought. It provides the type of elements plus an unstandardized but quick concentration for one or more elements in the specimen [19, 20]. The erosion mechanisms of the electrodes were thus determined from the above characterization.

2.5. Statistical analysis

In this work, we assumed that all experimental data are normally distributed. A statistical methodology sequence was applied to compare the mean of collected data using hypothesis testing as shown in Fig. 3 [21]. First, the test for equality of variance of several data was examined using Levene's test. If all variances were not statistically different, analysis of variance (ANOVA) for comparing several means of the experimental data was then used. Otherwise, two types of T-tests were used for pair-wise comparison, depending on the equality of variance of each pair. The F-test was used to

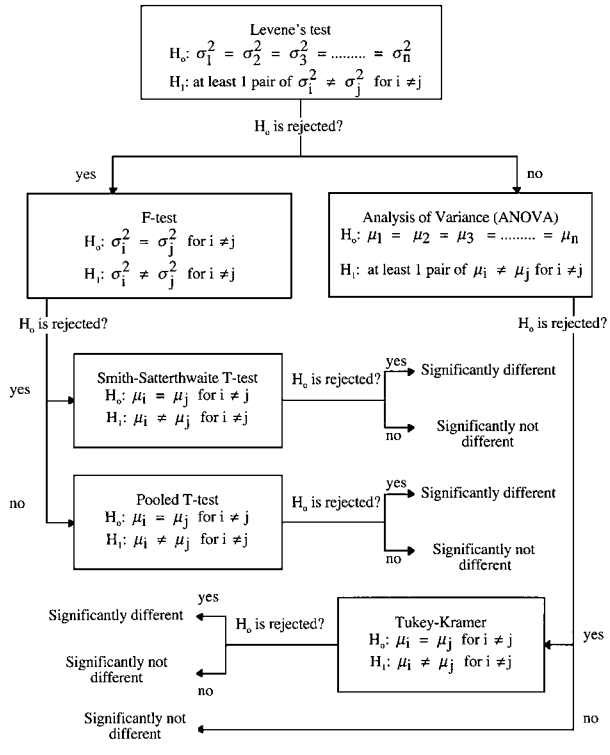

Figure 3 Flow chart of statistical analysis methodologies used in experimental comparison, with a confidence level of at least 95% or above; (μ) mean, (σ^2) variance of the data.

compare the variance of each pair. When the F-test yielded a significantly different variance, the Smith–Satterthwaite T-test was used. If not, the pooled T-test was used. In addition, although ANOVA results tell us whether several means of the data are significantly different or not, we could not tell which data pair were exactly different with such statistical differences. Thus, a further statistical comparison procedure, the Tukey–Kramer test, was necessary. All the above statistical analysis methods were used at a significant level of at least 95% or above. Moreover, for repeated experiments, the standard error or variance of each datum point was calculated.

3. Results

The data collected from repeated experiments, for copper, graphite and ZrB_2-Cu 1700, were found to have a standard error within the confidence level of 95% or above. Because of these results and experimental time limitations, we conducted only one experiment for ZrB_2-Cu, with the assumption that the standard error of this experiment would also be of a 95% confidence level. Considerable additional data, more than 200 experiments, were collected by the lead author, but not discussed here.

In addition, the differences between experimental data of different conditions are stated as the statistical difference with a confidence level of 95% or above. Oppositely, whenever we state that they are the same, this means that comparison of these data using the statistics yields an insignificant difference with a confidence level of 95% or above.

3.1. Effect of on-time and current on ZrB_2-Cu electrode performance

3.1.1. Workpiece (steel) removal rate

Fig. 4 shows the effect of varying on-time and current on the workpiece removal rate (WRR) when a ZrB_2-Cu 1700 electrode is used as the tool. The longer the on-time, the longer the spark stays on the surface of the steel and the higher the number of positive ions that can move towards the cathode surface. This causes a larger melted crater steel cavity, resulting in higher WRR. The energy input into this cathode workpiece is from positive ion bombardment. However, after a certain on-time (180 μs), the WRR reaches a steady state with a maximum value. This is due to limitation of the total amount of positive charges moving towards the cathode surface. This phenomenon also results in an almost constant volume of melted cavities. Accordingly, after a long on-time (320–560 μs), the WRR starts to decrease due to a longer on-time without further erosion of the cathode material and inefficient flushing during the off-time. Since the off-time (100 μs) is much lower than the on-time (320–560 μs), the debris is not removed or flushed out completely during the off-time. This causes the remaining debris to refreeze back on the surface, reducing the WRR. The incomplete flushing hypothesis was confirmed by comparing the WRR at two off-times of 100 and 240 μs both with a constant on-time of 560 μs. The WRR at an off-time of 240 μs is larger than that at 100 μs, and it is the same as the WRR at an on-time of 320 μs. The longer off-time of 240 μs allowed more debris to be flushed, causing more new non-eroded material on the surface to be melted and removed when the next spark hits the surface. In addition, the WRR increased with current owing to higher power input of the sparks into the steel surface.

3.1.2. Tool removal rate

The effect of on-time on tool removal rate (TRR) is different from that on WRR, as shown in Fig. 5. At the start of the spark, positively charged particles slowly migrate to the cathode workpiece, whereas the electrons rapidly move to the surface of the anode tool.

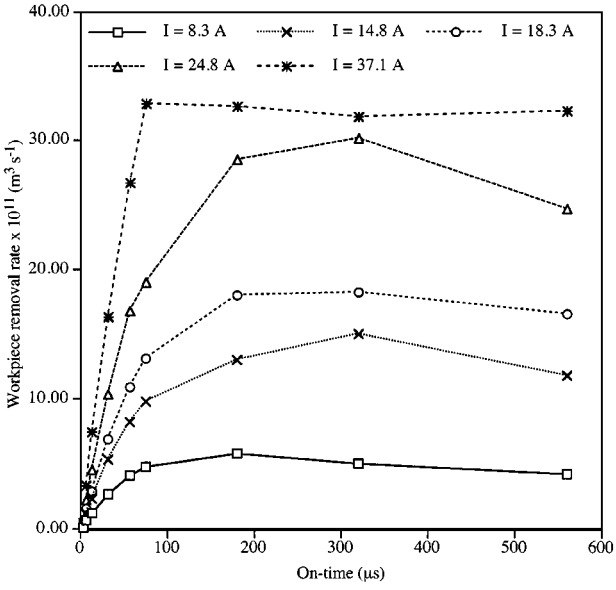

Figure 4 Workpiece (steel) removal rate with varied on-times and currents at a constant off-time of 100 μs. ZrB_2-Cu 1700 is the anode electrode.

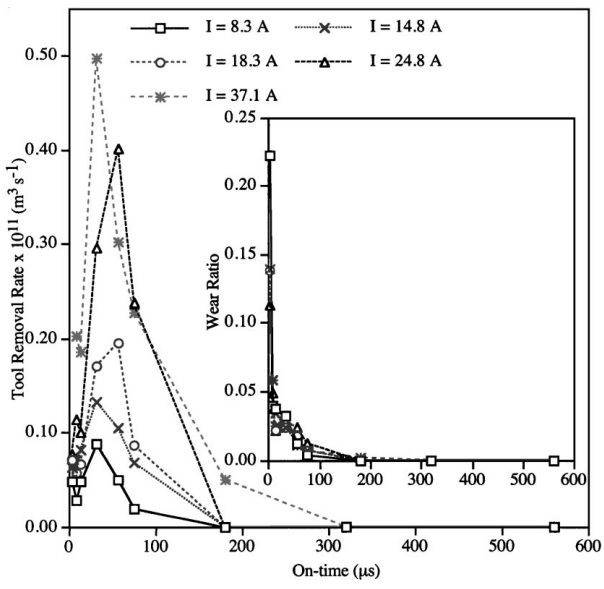

Figure 5 Removal rate of ZrB_2-Cu 1700 electrode and its wear ratio with varied on-times and currents at a constant off-time of 100 μs. Steel is the cathode workpiece.

This is because the electrons are much smaller and lighter than positive ions, and electrons avalanche near the anode surface. The anode first then begins to melt rapidly due to absorption of fast moving electrons. However, it resolidifies after a few microseconds due to lateral movement of electrons near the anode surface. This movement causes an expansion of the plasma channel at the anode surface, and hence reduction of the localized heat flux. Consequently, the TRR is decreased with increasing on-time. However, this phenomenon is not important at low on-times, as explained below.

From Fig. 5, at low on-time (3.2–56 μs), electrons do not have sufficient time to move laterally. However, the number of electrons moving towards the anode surface increases with on-time. This results in only a slight reduction of the heat flux, and, hence, an increase in the TRR. The TRR values at on-times of 7.5 and 13 μs for a current of 24.8 A, and those at on-times of 3.2 and 7.5 μs for all other currents, are considered to be comparable due to the random error of the experiment with a level of confidence of 95%. On the other hand, at on-times ranging from 56 to 560 μs, the plasma channel expands enough to reduce the localized heat flux. Accordingly, the TRR is decreased with increasing on-time, and no erosion of the electrode occurs.

In addition, there is the deposition of the melted and/or evaporated workpiece on the surface of the tool at all on-times. We confirm this deposition using the EDX. Fig. 6 is one of the EDX results of EDM ZrB_2-Cu anode electrode, in which the EDM conditions are a current of 14.8 A, an on-time of 56 μs and an off-time of 100 μs. At the end of the on-time, violent collapse of the plasma channel and a vapour bubble occurs. This causes the superheated, molten liquid on the surface of the steel to explode into the liquid dielectric. Some of this material is carried away by the dielectric, but some of it resolidifies on the workpiece and tool surfaces. It deposits on the workpiece surface due to the low temperature of the surface during the off-time, whereas violent explosion, within a very short gap between both workpiece and tool, causes deposition on the tool surface. Moreover, the surface temperature of the ZrB_2-Cu tool is lower than that of the steel workpiece, enhancing the refreezing and deposition of steel on the tool surface. This is due to the difference between the melting point of the tool and the workpiece. For the tool, Cu (1358 K) has a lower melting point than ZrB_2 (3300 K); consequently, most of the heat is conducted through Cu instead of ZrB_2. This results in almost no erosion of ZrB_2, and the surface temperature of the overall surface of the tool is hence approximately the melting point of Cu. On the other hand, for the steel workpiece the melting points of Fe (1804 K), Cr (2130 K) and Ni (1726 K) are higher than that of S (394 K). However, most of the heat is carried away by Fe owing to trace amounts of S, Cr and Ni. This causes the surface temperature of the workpiece to be nearly the melting point of Fe, which is also higher than that of Cu. In addition, EDX spectra of EDM ZrB_2-Cu (not shown), when reverse polarity is applied, reveal the deposition of Fe, Cr, Ni and S on the ZrB_2-Cu electrode. The condition of reverse polarity is when steel is the anode and ZrB_2-Cu is the cathode. The result assures that the surface temperature of ZrB_2-Cu is lower than that of steel. We also find from Fig. 5 that the TRR is increased with current due to higher power input into the electrode surface.

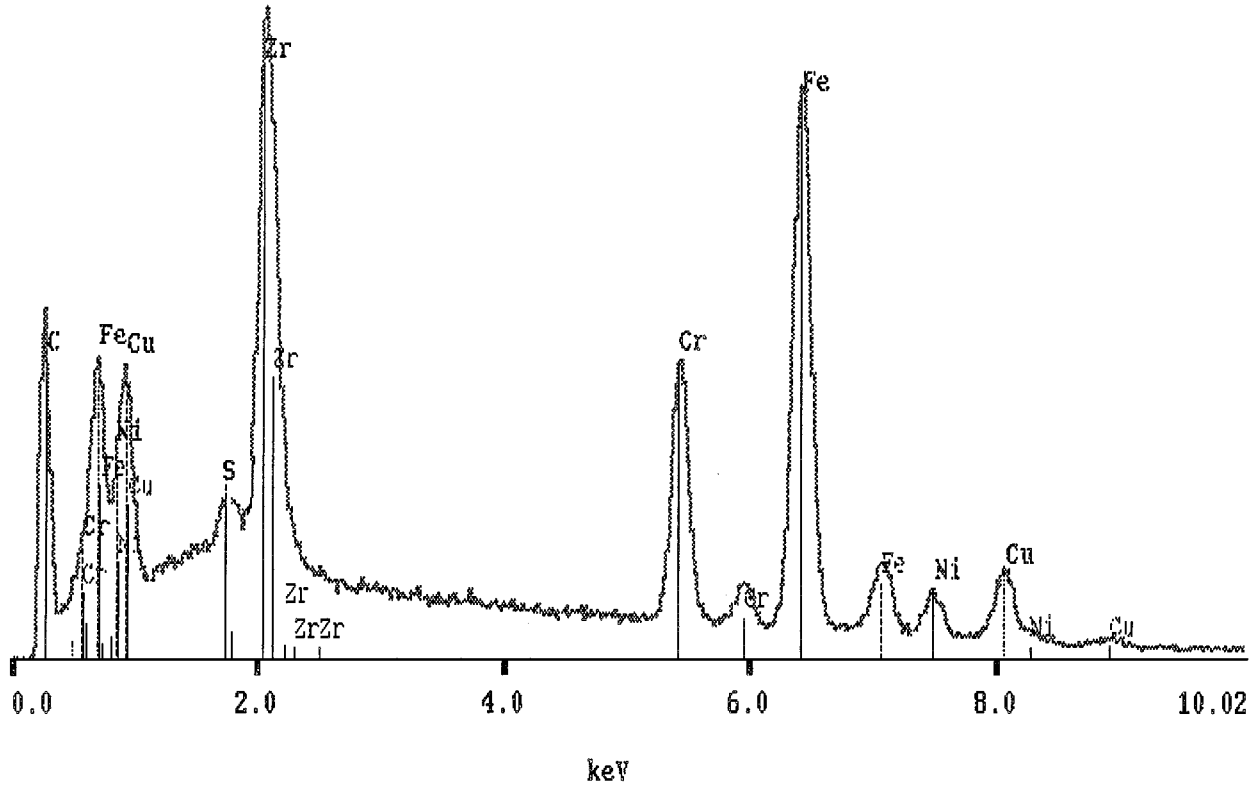

Figure 6 EDX spectrum of the EDM ZrB_2-Cu ART tool. The conditions of EDM are: current, 14.8 A; on-time, 56 μs; off-time, 100 μs.

3.1.3. Wear ratio of tool removal rate to workpiece removal rate

Fig. 5 also shows the wear ratio of TRR to WRR as a function of on-time for various currents. At low on-times, TRR and WRR are increased with increasing on-time, but TRR is much lower than WRR. Thus, wear ratio (WR), or TRR divided by WRR, decreases with increasing on-time. At high on-times, the WRR reaches a maximum value while the TRR decreases with increasing on-time. Accordingly, the WR decreases with increasing on-time. The WR increases with increasing current due to higher power input when the current is increased.

3.1.4. Surface roughness of workpiece and tool

Figs. 7 and 8 show the surface roughness after EDM of the workpiece (steel) and tool (ZrB_2-Cu 1700 electrode), respectively, with increasing on-time for various currents.

Positive ion bombardment increases with increasing on-time, resulting in bigger melt cavities and rougher surfaces of the cathode. The volume of the cathode's melt cavities is finally constant; thus, the surface roughness of the workpiece reaches a steady state after a certain on-time, as shown in Fig. 7. Moreover, power input increases with higher current, causing a bigger crater of the melted steel cavity and thus rougher surfaces.

Unlike the workpiece, two different mechanisms occur at the tool surface when we increase on-time. From Fig. 8, at low on-times (3.2–56 μs), electron bombardment with low plasma channel expansion occurs, causing erosion of the anode electrode to be the dominant mechanism. Electron bombardment increases with increasing on-time, resulting in rougher surfaces. At on-times ranging from 56 to 180 μs, resolidification of the melted electrode occurs due to expansion of the plasma channel. This causes smoother surfaces. On the contrary, at high on-times (180–560 μs), no erosion of anode material occurs due to very high plasma channel expansion, and erosion of the workpiece increases with increasing on-time. This results in an increase in the deposition of melted and/or evaporated steel on the anode electrode's surface, and thus to rougher surfaces.

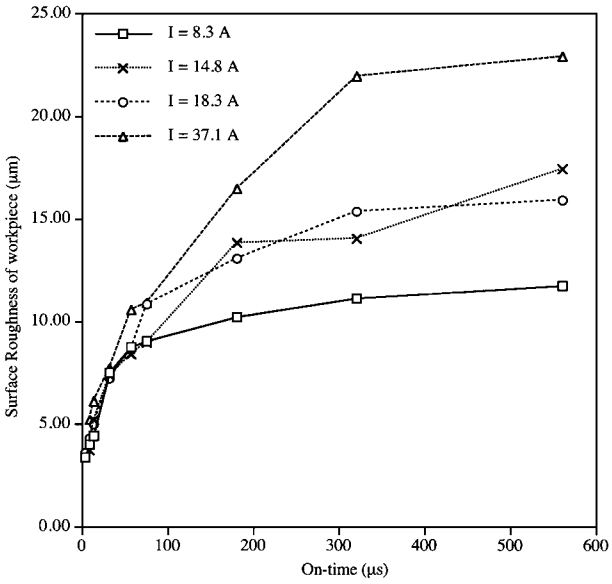

Figure 7 Surface roughness of steel workpiece with varied on-times and currents. ZrB_2-Cu 1700 electrode is the tool.

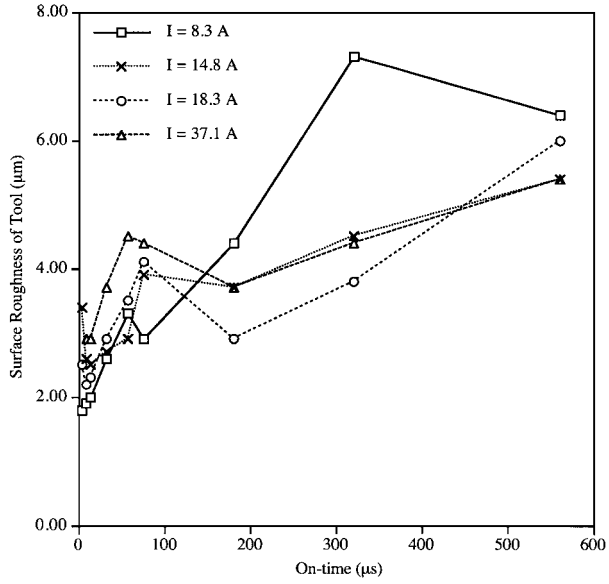

Figure 8 Surface roughness of ZrB_2-Cu 1700 electrode tool with varied on-times and currents. Steel is the workpiece.

3.2. Performance comparison of ZrB_2-Cu electrode to Cu and graphite electrodes

3.2.1. Workpiece (steel) removal rate

Fig. 9 shows the steel removal rate (WRR) with increasing on-times for various types of tools when a current of 14.8 A and an off-time of 100 μs are applied. There are four types of tools including Cu, graphite, ZrB_2-Cu 1700 and ZrB_2-Cu ART.

The WRRs are comparable for both ZrB_2-Cu 1700 and ZrB_2-Cu ART electrodes. We hence conclude that different types of infiltrated Cu have little effect on the WRR. Except for on-times ranging from 320 to 560 μs, both ZrB_2-Cu 1700 and ZrB_2-Cu ART yield

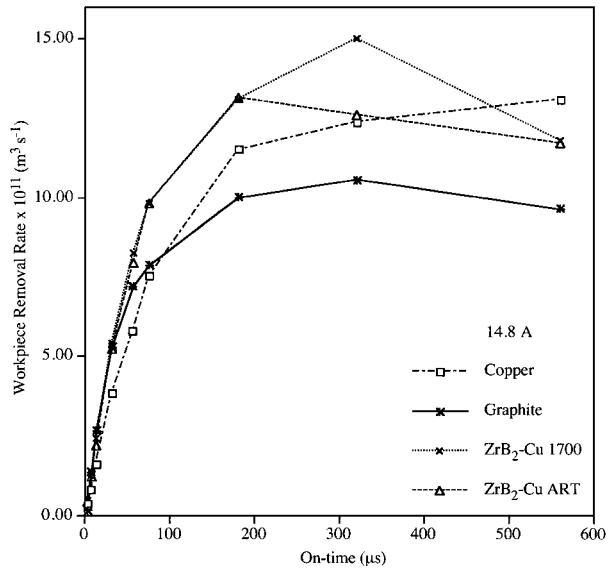

Figure 9 Comparison of steel removal rate using different tools at a current of 14.8 A and an off-time of 100 μs.

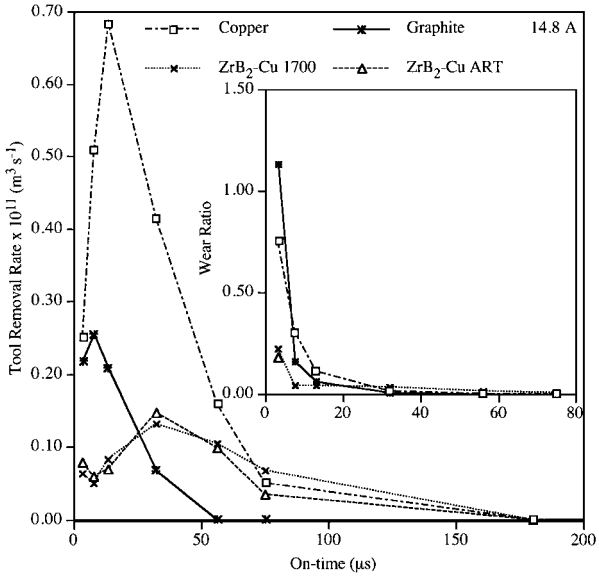

Figure 10 Removal rates of various tools and their wear ratios at a current of 14.8 A and an off-time of 100 μs. Steel is the workpiece.

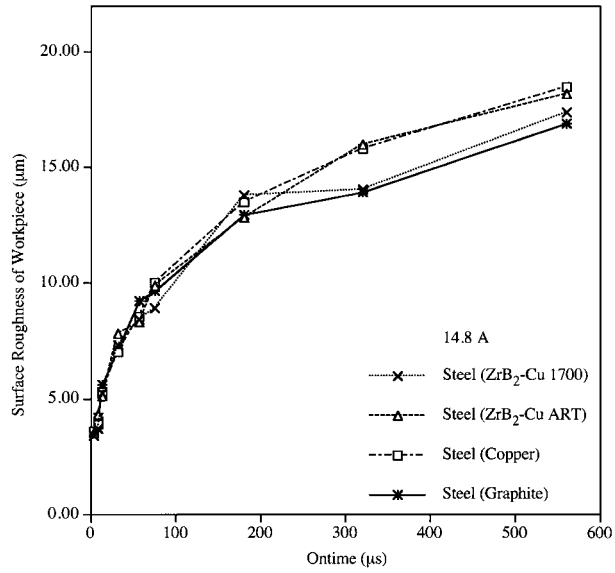

Figure 11 Surface roughness of steel as a function of the type of tools at a current of 14.8 A and an off-time of 100 μs.

the highest WRR compared with Cu and graphite. The normal range of on-times used in most industries is from 10 to 180 μs. Consequently, for commercial applications, use of composite electrodes leads to a higher yield of cutting workpiece materials. Again, the decrease in WRR at high on-times (320–560 μs) is due to the constant volume of the melt cavities with increasing on-times.

3.2.2. Tool removal rate

Fig. 10 shows the removal rate of all four electrodes (TRR) when steel is the cathode workpiece at a current of 14.8 A and an off-time of 100 μs.

The removal rates of both ZrB_2-Cu 1700 and ZrB_2-Cu ART are comparable, assuring the unimportance of the type of infiltrated Cu to the electrode and to EDM. In addition, it is of interest only to compare the TRR of different electrodes at low on-times up to 75 μs. This is because the TRRs of all electrodes are comparable and close to zero at high on-times (75–560 μs). The removal rate of copper is the highest in the low on-time range (3.2–75 μs). The TRR of graphite is the lowest at on-times ranging from 28 to 75 μs, whereas those of both ZrB_2-Cu 1700 and ZrB_2-Cu ART are the lowest at extremely low on-times (3.2–28 μs).

Accordingly, excellent wear resistance of composite electrodes at extremely high heat flux conditions (very low on-time) is appealing for their utilization for most plasma-related applications, such as micromachining.

3.2.3. Wear ratio of tool removal rate to workpiece removal rate

For EDM applications, the ZrB_2-Cu tool yields the most effective and productive cutting. Although the TRR of graphite is lower than that of both ZrB_2-Cu 1700 and ZrB_2-Cu ART over a certain range of on-times (20–75 μs), the WRRs of the composite electrodes are the highest, resulting in the lowest wear ratio as shown in Fig. 10.

3.2.4. Surface roughness of workpiece (steel)

In EDM applications, the finishing condition is critical to the final product's surface quality. The finishing condition is when the current and on-time are low, producing shiny and ultrasmooth surfaces. A study of the effect of the type of tool on the workpiece's surface quality shows that it is not important to surface quality at the finishing conditions shown in Fig. 11. Also, for a required surface quality, we can identify from this figure the EDM machine setting required when using a ZrB_2-Cu tool.

4. Discussion

In order to understand why this composite electrode has a lower wear rate than other electrodes, electron microprobe analysis, SEM and EDX were employed to study the erosion mechanism. The SEM image of the EDM ZrB_2-Cu tool accompanied by the identification of elements using EDX (not shown here) show that Cu recesses while molten ZrB_2 resolidifies back to the original position. Some molten ZrB_2 also flows down into the Cu recesses and smears on top of the copper matrix. Also, steel materials (Fe, Cr, Ni and S) deposit all over the surface of the ZrB_2-Cu tool. The small balls deposited on the surface of the EDM ZrB_2-Cu tool are resolidified steel materials.

X-ray elemental mapping using the electron microprobe provides the location of Cu, ZrB_2, Fe and Cr on the surface subjected to EDM. Fig. 12 shows the inverted elemental map of this electrode. Fig. 12a is a SEM image of the area of surface subjected to EDM where the microprobe electron beam strikes. The dark spots in Fig. 12b–f represent the location of B, Cu, Zr, Cr and Fe, respectively. We found that most Cu is located in the deep holes, and a little Cu appears in the recessed plane. Contrarily, molten ZrB_2 resolidifies and forms a plateau on top of the original ZrB_2 matrix, and some molten ZrB_2 flows into the recessed Cu and resolidifies there.

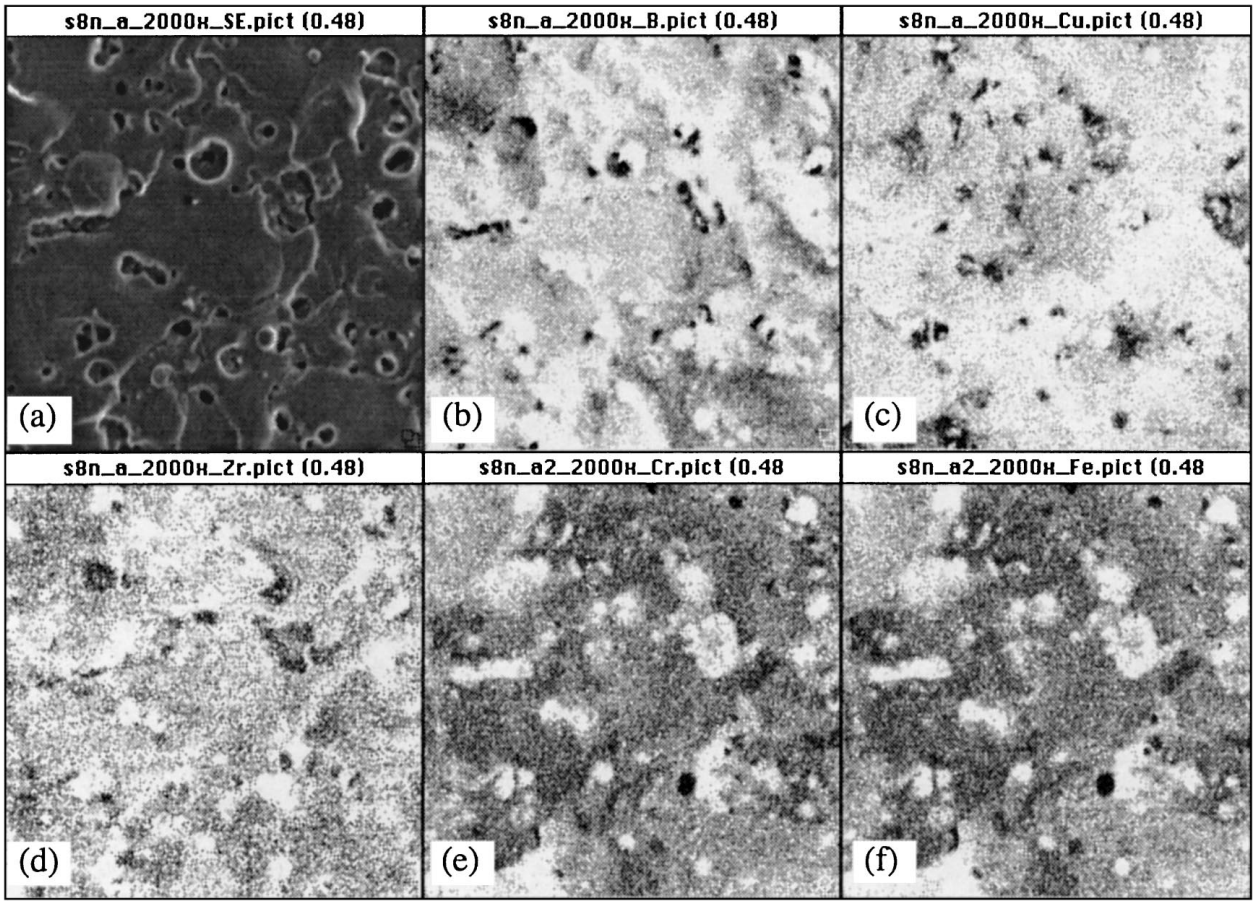

Figure 12 An inverted elemental mapping of EDM ZrB_2-Cu ART at a current of 4.0 A, an on-time 3.2 μs and an off-time of 100 μs; steel is the workpiece. (a) SEM image of EDM surface ($\times$1570 magnification); X-ray maps of (b) B, (c) Cu, (d) Zr, (e) Cr and (f) Fe, respectively.

The above results indicate that Cu has significantly melted and/or evaporated, while most ZrB_2 has melted and thermal spalled. The thermal spalling of ZrB_2 is observed by the flat surface of the ceramic phase after cooling at the end of EDM. Accordingly, most of the heat is carried away through the Cu matrix, reducing the thermal stress and lowering the surface temperature in the ZrB_2 phase. The molten Cu thus tends to refreeze quickly back near the ceramic matrix surrounding the Cu phase. Moreover, when the sparks strike the smeared ZrB_2 area on top of the recessed Cu, thermal spalling is prevented by the high thermal conductivity of the metal phase underneath the ceramic matrix. This also enhances the resistivity of wear of this composite material. Consequently, the combination of dominant melting and evaporation of the metal phase, negligible thermal spalling and melting of the ceramic phase, and quick refreezing of the metal phase causes the extremely low wear rate of this composite material. This erosion mechanism make the performance of the electrode superior to that of pure metal and ceramic electrodes. In EDM applications, metals normally erode by melting whereas ceramics erode by thermal stress and/or melting.

In addition, the deposition of Fe and Cr has also been discovered all over the electrode surface. This is due to the difference between the melting points of the tool and the workpiece as explained in the previous section. We also observe small balls of Fe and Cr deposited on the surface subjected to EDM as shown in Fig. 12. This supports the idea that violent explosion of steel debris occurs at the end of the on-time (the beginning of plasma collapse). This debris, in turn, is flushed away by the cold dielectric fluid surrounding the formerly existing plasma, resulting in refreezing of the molten debris. This molten debris tends to resolidify to spherical shape due to surface tension. However, complete flushing of the debris out of the small gap between both of the electrodes does not occur. It should be remembered that the electrode gaps are 20–300 μm, depending on the current, and the workpiece melt craters have diameters approaching these sizes. Thus, some of the spherical debris deposits on the surface of the tool. This deposition of workpiece material on the tool surface acts as the addition of new material onto the tool surface, reducing the total erosion rate of the tool after finishing EDM.

5. Conclusions

We used a conventional method to synthesize ZrB_2-Cu electrodes, starting from (i) mechanical pressing of polymer-coated ZrB_2 powders, and (ii) infiltration of copper into the green body in a high-temperature furnace. The way to control the amount of infiltrated copper is to vary the pressure of the press. The higher the pressure, the lesser the voids between the particles, reducing the amount of copper required to infill the voids.

However, the copper tends to fill the voids incompletely, since its infiltration is mainly due to the flow of molten liquid copper opposing the capillary force inside the voids. Consequently, this method might not be the best way of manufacturing the electrode since it is difficult to predict the concentration of copper in the electrode. However, we found that the ZrB_2-Cu electrode has the highest thermal wear resistance to the plasma spark at the condition of extremely high energy flux (at low on-time). Also, the electrode could cut the steel workpiece faster than graphite- and copper-shaping tools. Consequently, this electrode should have an impact on thermal plasma industries.

Due to the large difference between the melting point of the copper phase and that of the ZrB_2 phase, the erosion mechanism of the electrode is different from that of the pure elemental electrode. The difference in the type of infiltrated copper is thus not important to the performance of the electrode as long as the melting point of the copper is well below that of the ZrB_2 phase.

Moreover, the complete data bank of WRR, TRR, wear ratio and surface quality over a wide range of on-times for ZrB_2-Cu electrodes can be used as a reference to find the operating condition for a required surface quality and workpiece removal rate.

Acknowledgements

We would like to acknowledge the full financial support of the National Science Foundation, grant DMR 9420386. We are grateful to Advanced Refractory Technologies, Inc. (ART) for co-operation in preparing the electrodes. Also, our appreciation is extended to Dr R. N. Guillemette for his effort and technical suggestions to the analysis of these materials.

References

1. M. I. BOULOS, P. FAUCHAIS and E. PFENDER, in "Thermal Plasma Fundamentals and Applications" (Plenum Press, New York, 1994) pp. 33–48.
2. J. E. HARRY, *J. Appl. Phys*. **40** (1969) 265.
3. A. MAROTTA, *J. Phys. D, Appl. Phys*. **27** (1994) 49.
4. J. R. FENTER, *Sampe Quarterly* **2** (1971) 1.
5. B. ISE, S. MEGURO, T. TAMURA and O. TAKAGI, *TohoKu Kogya Daigaku Koyo* **1** (1988) 25.
6. Y. M. CHENG, P. T. EUBANK and A. M. GADALLA, *Mater. Manufac. Processes* **II** (1996) 565.
7. Y. M. CHENG and A. M. GADALLA, *ibid*. **II** (1996) 575.
8. A. M. GADALLA, B. BOZKURT and N. M. FAULK, *J. Amer. Ceram. Soc*. **74** (1991) 801.
9. P. C. PANDEY and H. S. SHAN, in "Modern Machining Processes" (McGraw-Hill, New York, 1981) p. 85.
10. T. O. HOCKENBERRY and E. M. WILLIAMS, *IEEE Trans. Ind. Gen. Appl.* **IGA-3** (1967) 302.
11. C. V. OSENBRUGGEN, *Phillips Tech. Rev*. **30** (1969) 195.
12. M. R. PATEL, M. A. BARRUFET and P. T. EUBANK, *J. Appl. Phys*. **66** (1989) 4104.
13. D. D. DIBINTOTO, P. T. EUBANK and M. A. BARRUFET, *ibid*. **66** (1989) 4095.
14. J. W. ROBINSON, *ibid*. **38** (1967) 210.
15. J. W. ROBINSON, M. HAM and A. N. BALASTER, *ibid*. **44** (1973) 72.
16. J. W. ROBINSON, *ibid*. **44** (1976) 210.
17. P. T. EUBANK, M. R. PATEL, M. A. BARRUFET and B. BOZKURT, *ibid*. **73** (1993) 7900.
18. Federal Products Corporation, in "Surfanalyzer System 5000/400 User's Manual" (August 1991).
19. K. L. WILLIAMS, in "An Introduction to X-Ray Spectrometry" (Allen & Unwin, Winchester, MA, 1987) p. 129.
20. E. P. BERTIN, in "Introduction to X-Ray Spectrometric Analysis" (Plenum Press, New York, 1978) pp. 439–44.
21. J. S. MILTON and J. C. ARNOLD, in "Introduction to Probability and Statistics: Principles and Applications for Engineering and the Computing Sciences," 3rd Edn, (McGraw-Hill, New York, 1995).

Received 23 December 1997
and accepted 29 July 1998